# Isotopic effects in the interaction of $O^-$ with $D_2$ and $H_2$ at low temperatures

Radek Plašil,* Thuy Dung Tran, Štěpán Roučka, Pavol Jusko, Dmytro Mulin, Illia Zymak, Serhiy Rednyk, Artem Kovalenko, Petr Dohnal, and Juraj Glosík
*Department of Surface and Plasma Science, Faculty of Mathematics and Physics, Charles University, Prague, Czech Republic*

Karel Houfek, Jiří Táborský, and Martin Čížek
*Institute of Theoretical Physics, Faculty of Mathematics and Physics, Charles University, Prague, Czech Republic*
(Received 3 October 2017; published 7 December 2017)

The isotopic effects in reactions of $O^-$ ions with $H_2$ and $D_2$ have been studied experimentally using a cryogenic 22-pole radio-frequency ion trap. The rate coefficients for associative detachment leading to $H_2O + e^-$ and to $D_2O + e^-$ and for atom transfer reactions leading to formation of $OH^-$ and $OD^-$ ions were determined at temperatures ranging from 15 to 300 K. The measured temperature dependencies of the rate coefficients for both channels of reactions of $O^-$ with $H_2$ and $D_2$ are compared with the results of the classical trajectory Monte Carlo simulation of the $O^- + H_2$ and $O^- + D_2$ collisions using the newly calculated potential energy surfaces. The measured temperature dependencies of the reaction rate coefficients for associative detachment are in very good agreement with the calculated ones. Agreement between experimental and calculated temperature dependencies of the rate coefficients of atom transfer reactions is off at most by a factor of 3 and the isotope effect is reproduced.

DOI: 10.1103/PhysRevA.96.062703

## I. INTRODUCTION

The reaction of $O^-$ with $H_2$ or $D_2$ has two exothermic channels corresponding to associative detachment (AD) and hydrogen or deuterium atom transfer (AT) [channels (1) and (2) for hydrogen or (3) and (4) for deuterium]:

$$O^- + H_2 \xrightarrow{k_1} H_2O + e^-, \quad \Delta H = -3.57\ \text{eV}, \tag{1}$$

$$O^- + H_2 \xrightarrow{k_2} OH^- + H, \quad \Delta H = -0.30\ \text{eV}, \tag{2}$$

$$O^- + D_2 \xrightarrow{k_3} D_2O + e^-, \quad \Delta H = -3.65\ \text{eV}, \tag{3}$$

$$O^- + D_2 \xrightarrow{k_4} OD^- + D, \quad \Delta H = -0.28\ \text{eV}, \tag{4}$$

with the reaction rate coefficients $k_1$, $k_2$, $k_3$, and $k_4$, respectively. The reaction enthalpies at 0 K were calculated from bond dissociation energies [1,2] and electron affinities [3–5] and corrected for zero-point energy differences in case of the deuterated reactions [6–8]. The endothermic proton or deuteron transfer channel in which $H^- + OH$ or $D^- + OD$ is formed with $\Delta H = 0.77$ or 0.79 eV, respectively, does not play a role in the present low temperature experiments.

Since hydrogen and oxygen are among the most abundant elements in the Universe, the studied reactions are also astrochemically relevant. In particular, associative detachment contributes to formation of water in the interstellar medium [9], which is a fundamental problem in astrochemistry tightly related to the origin of terrestrial water [10–12]. Knowledge of gas-phase processes involving water [13] and especially those leading to isotopic fractionation [12,14] appears to be crucial for understanding water formation in space.

In low-energy collisions of reactants in the ground electronic states, $O^-(^2P) + D_2(X\,^1\Sigma_g^+)$, the collision system has three accessible electronic states $1^2A'$, $1^2A''$, and $2^2A'$ (as in collisions of $O^-$ with $H_2$). For better orientation, one-dimensional cuts of the calculated potential energy surfaces (PES) of $D_2O^-$ and $D_2O$ along the minimum energy path going from $O^- + D_2$ to $OD^- + D$ on the $1^2A'$ PES are shown in Fig. 1. Plotted are also cuts through the PES calculated for $1^2A''$ and $2^2A'$ states along the same coordinate. Autodetachment towards $e^- + D_2O$ can occur in the region where the anionic curve is above the neutral one. For further details see also [15,16] where features of the PES including a local minimum on the $1^2A'$ surface were discussed.

The $O^-$ ion can be present in two fine structure states $O^-(^2P_{\frac{1}{2}})$ and $O^-(^2P_{\frac{3}{2}})$ which are separated by 22 meV [17,18]. We assume that the ratio of population of the $O^-(^2P_{\frac{1}{2}})$ and $O^-(^2P_{\frac{3}{2}})$ states is 1:2, which corresponds to statistical probability of production in the ion source. We do not expect that this ratio will be changed in collisions with helium buffer gas, which is used to thermalize ions injected into the trap [19]. Collisions with $H_2$ or $D_2$ also cannot contribute to a change of the ratio, since at low temperature the reactions proceed with nearly collisional rate, i.e., almost every collision of $O^-$ with $H_2$ or $D_2$ is reactive.

Molecules $H_2$ and $D_2$ can be in a para or ortho nuclear spin configuration. The ground state of $H_2$ is para-$H_2$ and the ground state of $D_2$ is ortho-$D_2$. In the present experiments we are using normal hydrogen and normal deuterium gases, where the populations of ortho and para states correspond to thermal equilibrium at 300 K, which is close to the statistical ratio 1/3 for para-$H_2$/ortho-$H_2$ and 1/2 for para-$D_2$/ortho-$D_2$. Our experiments have indicated that para- or ortho-$H_2$ populations do not change while passing the reactant gas from a reservoir into the trap volume [20,21] and we expect that the same will hold for $D_2$.

Experimental studies of the reactions (1), (2), (3), and (4) and the temperature dependencies of their rate coefficients have been carried out by other groups at room temperature

*radek.plasil@mff.cuni.cz

 

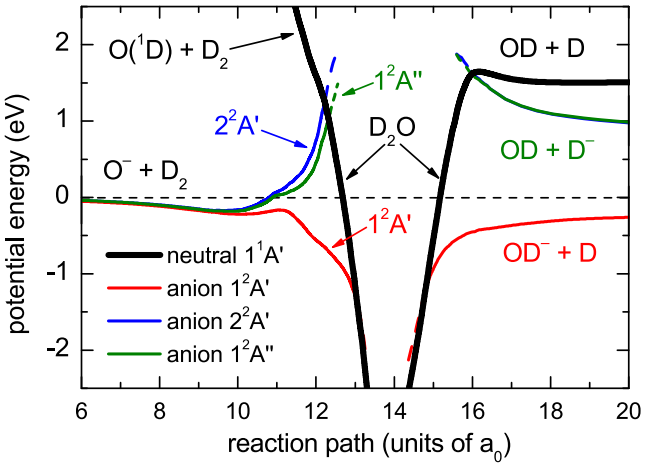


FIG. 1. The calculated potential energy surfaces (PES) of $D_2O^-$ and $D_2O$ along the minimum energy path going from $O^- + D_2$ to $OD^- + D$ on the $1^2A'$ PES. Plotted are also the PES corresponding to the $1^2A''$ and $2^2A'$ states, which are connected to the $OD + D^-$ asymptote. The PES of $D_2O^-$ in the autodetachment region are indicated by dashed lines. For further details see also [15].

and above using flowing afterglow, drift tube, tandem mass spectrometry, and octopole ion trap instruments (see, e.g., Refs. [22,23] and references therein). A study at mean collision energies down to 0.02 eV has been carried out by Viggiano *et al.* [24] using a temperature variable flow-drift tube. The isotope effects on the product energy partitioning in the atom transfer reaction have been studied by Lee and Farrar [25]. The kinetic energy distribution of electrons produced in associative detachment has been studied by Mauer and Schulz [26], Esaulov *et al.* [27], and most recently by Jusko *et al.* [23]. All these studies of AD indicate production of low-energy electrons and high internal excitation of the produced $H_2O$ or $D_2O$ molecules.

The intermediate $H_2O^-$ or $D_2O^-$ complex has been studied theoretically [28,29] and experimentally [30–33] by means of dissociative electron attachment to the neutral $H_2O$ or $D_2O$ molecule at energies 6–12 eV. The detailed potential energy surfaces of the lowest $H_2O$ and $H_2O^-$ states have been calculated by Claydon *et al.* [34], Werner *et al.* [35], and newly by Houfek and Čížek [16].

To our knowledge, there are no measured rate coefficients of the reaction of $O^-$ with $D_2$ for temperatures below 170 K, despite the fact that temperatures down to 10 K are typical for interstellar molecular clouds [12,13,36]. The rate coefficients of the reaction of $O^-$ with $H_2$ were recently studied in our laboratory in the temperature range 10–300 K [15] and we measured the energy distribution of electrons produced in associative detachment of $O^-$ with $H_2$ and $D_2$ [reactions (1) and (3)] at 300 K and the corresponding rate coefficients [23].

We present an extended study of the reaction of $O^-$ with $D_2$ down to 15 K. We report the measured temperature dependencies of the rate coefficient of associative detachment [reaction (3)] and of deuterium atom transfer [reaction (4)]. Although this work is focused on the interaction of $O^-$ with $D_2$, we also present newly measured rate coefficients of the reactions (1) and (2) with significantly improved accuracy compared to those of Jusko *et al.* [15]. We also report the calculated rate coefficients of AD and AT in collisions of $O^-$ with $H_2$ and $D_2$ and we discuss the observed isotope effect.

## II. EXPERIMENT

The reaction of $O^-$ ions with $H_2$ or $D_2$ was studied using the cryogenic 22-pole radio-frequency ion trap. As the detailed description of the instrument can be found elsewhere [37–41], only a very short description will be given here. Primary $O^-$ ions were produced in the storage ion source by electron bombardment of $N_2O$. In the standard procedure the anions are extracted from the ionization chamber of the ion source, mass selected, and injected into the ion trap. The anions injected into the trap are thermalized in collisions with helium buffer gas and react with $H_2$ or $D_2$ reactant gas. The trap is cooled by a cryocooler reaching temperatures down to 10 K. Due to low $H_2$ or $D_2$ density in comparison with helium density (the ratios $[H_2]/[He]$ and $[D_2]/[He]$ are $\approx$0.01) we expect thermalization of kinetic energy of $O^-$ prior to their reaction. The thermalization of trapped ions was studied in many experiments and in the present work it can be assumed that the kinetic temperature $T$ of $O^- + H_2$ or $D_2$ collisions typically deviates from the nominal trap temperature $T_{22PT}$ by +5 K, i.e., $T = T_{22PT} + (5 \pm 5)$ K (for more details see Refs. [21,40,42]). After preselected storage (reaction) time $t$ the stored primary and product ions are extracted from the ion trap, mass selected by the second quadrupole mass spectrometer, and counted by the detector system with a microchannel plate. On the basis of the experimental data we assume that the number of detected ions is proportional to the number of trapped ions and that the detection efficiency is the same for $O^-$, $OH^-$, and $OD^-$. From measured dependencies of relative numbers of detected anions on the storage time, the reaction rate coefficient, and the branching ratio are determined.

In order to determine the pressure $p_{22PT}$ in the trap, the pressure $p_{SRG}$ measured using a calibrated spinning rotor gauge at room temperature $T_{room}$ connected directly to the trap volume is corrected for thermal transpiration using the formula

$$p_{22PT} = p_{SRG}\sqrt{T_{gas}/T_{room}}. \quad (5)$$

The systematic uncertainty of the reactant gas number density due to accuracy of pressure reading, stability of leak valves, and temperature dependence of vacuum conductivity of the trap is below 20%. In addition, the uncertainty of the gas temperature also contributes to the uncertainty of number density due to thermal transpiration (5).

## III. EXPERIMENTAL RESULTS

The measured time dependencies of numbers of trapped anions were analyzed by least-squares fitting with the following formulas obtained by integrating the kinetic equations. For the reaction with $D_2$ the formulas are

$$N_O(t) = N_O(0)\, e^{-(k_3+k_4)[D_2]t}, \quad (6)$$

$$N_{OD}(t) = N_{OD}(0) + N_O(0)\,(1 - e^{-(k_3+k_4)[D_2]t})\,\frac{k_4}{k_3+k_4}, \quad (7)$$

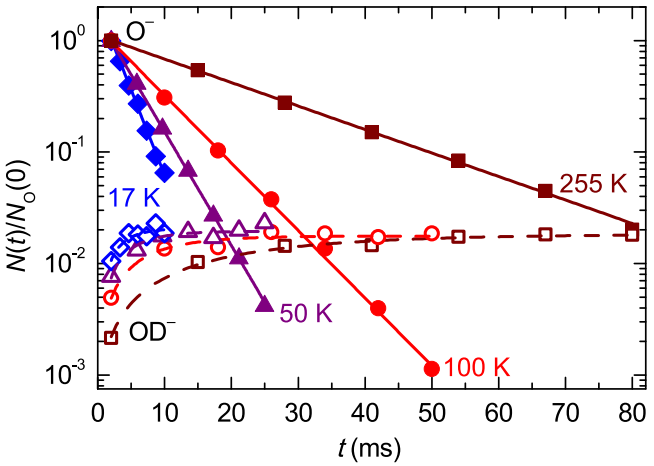


FIG. 2. Relative number of primary $O^-$ ions $N_O(t)/N_O(0)$ (full symbols) and $OD^-$ product ions $N_{OD}(t)/N_O(0)$ (empty symbols) at indicated trap temperatures as a function of storage time. The statistical error bars are smaller than the symbols. The fitted curves are indicated by lines. The $D_2$ number density is $3.1 \times 10^{11}$ cm$^{-3}$ at 17 K and it scales with $1/\sqrt{T}$ due to thermal transpiration.

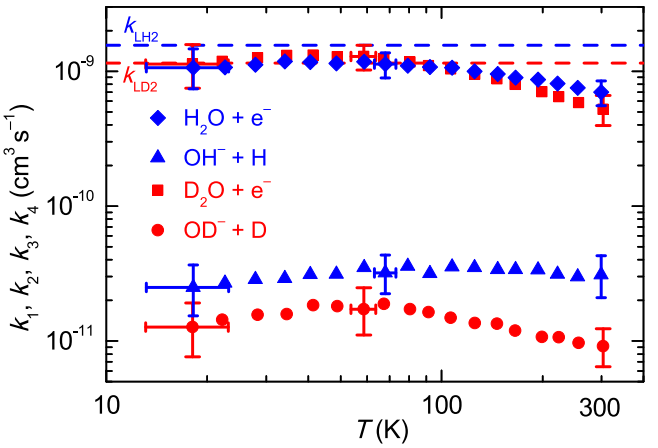


FIG. 4. Measured temperature dependencies of the rate coefficients of AD and AT reactions of $O^-$ with $H_2$ and $D_2$. The dashed horizontal lines are the Langevin rate coefficients $k_{LH2}$ and $k_{LD2}$ for the $O^- + H_2$ and $O^- + D_2$ collisions, respectively. The overall uncertainty is indicated for a few representative points by the error bars with caps.

where $k_3$ and $k_4$ are the respective reaction rate coefficients of the reactions (3) and (4), $N_O(t)$ and $N_{OD}(t)$ are numbers of the respective $O^-$ and $OD^-$ ions after storage time $t$, and $[D_2]$ is the deuterium number density in the trap volume. $N_O(0)$, $N_{OD}(0)$, $k_3$, and $k_4$ are free parameters of the fit. Good agreement of the fits with the measured data is illustrated in Fig. 2.

By varying the trap temperature, we were able to measure the reaction rate coefficients in the temperature range of 15–300 K. The loss of $O^-$ ions in pure helium without added $H_2$ or $D_2$ was negligible in the whole temperature range.

The binary character of the studied reactions can be seen from the dependence of the loss rate $r$ on the reactant gas number density. Examples of such dependencies for the reaction with deuterium are shown in Fig. 3. The linearity of these dependencies confirms that the loss of $O^-$ ions in the trap

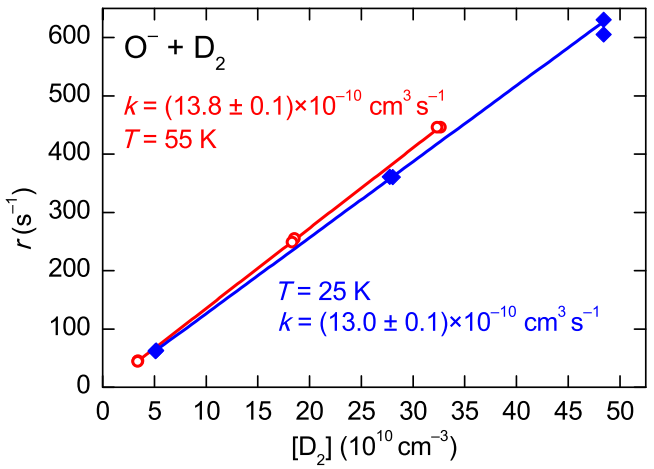


FIG. 3. The measured loss rate of $O^-$ as a function of $D_2$ number density at 25 and 55 K. The overall reaction rate coefficients $k = k_3 + k_4$ are given by the slope of the fitted linear dependencies.

is caused by the binary ion-molecule reaction with $D_2$, i.e., the rate can be expressed by the formula $r = (k_3 + k_4)\,[D_2]$.

The measured temperature dependencies of the rate coefficients $k_1$, $k_2$, $k_3$, and $k_4$ of the reactions (1), (2), (3), and (4) are shown in Fig. 4. We have to note that the rate coefficients for reactions with $H_2$ are approximately 40% lower in comparison with our previous low temperature experiment [15]. The difference between present and previous [15] data is higher than the estimated systematic uncertainties, which are 20% in both cases. As we found out, the systematic uncertainty in the previous work was underestimated, since it did not account for the nonlinearity of the ionization gauge in the trap vacuum chamber, which was calibrated using a spinning rotor gauge at moderate pressures ($\gtrsim 10^{-7}$ mbar) and used for measurement of pressure of the reactant gas ($\approx 10^{-8}$ mbar). Our recent experiments show that the nonlinearity in the relevant pressure range indeed reaches up to 40%. In order to eliminate this source of error in the present work, we have measured the reactant gas pressure using the spinning rotor gauge which is connected directly to the trap envelope. We have also checked that other experiments in our laboratory, which were using the same procedure for calibration of $H_2$ pressure [21,42], were not operated in the problematic pressure range of the ionization gauge and we have reproduced their results in experiments with direct measurement of reactant pressure.

In the covered range of temperatures, the measured temperature dependencies of the rate coefficients of reactions with $D_2$ ($k_3$ and $k_4$) are similar to those of reactions with $H_2$ ($k_1$ and $k_2$). To show possible influence of the difference in the mass of $H_2$ and $D_2$ on the reaction rate coefficients, we plotted in Fig. 5 the measured reaction rate coefficients $k_1$, $k_2$, $k_3$, and $k_4$ normalized to the corresponding Langevin collisional rate coefficients $1.56 \times 10^{-9}$ cm$^3$ s$^{-1}$ for $O^- + H_2$ and $1.15 \times 10^{-9}$ cm$^3$ s$^{-1}$ for $O^- + D_2$. From the plots in Fig. 5 it is clear that the difference in the Langevin collisional rate coefficients cannot simply explain the measured differences

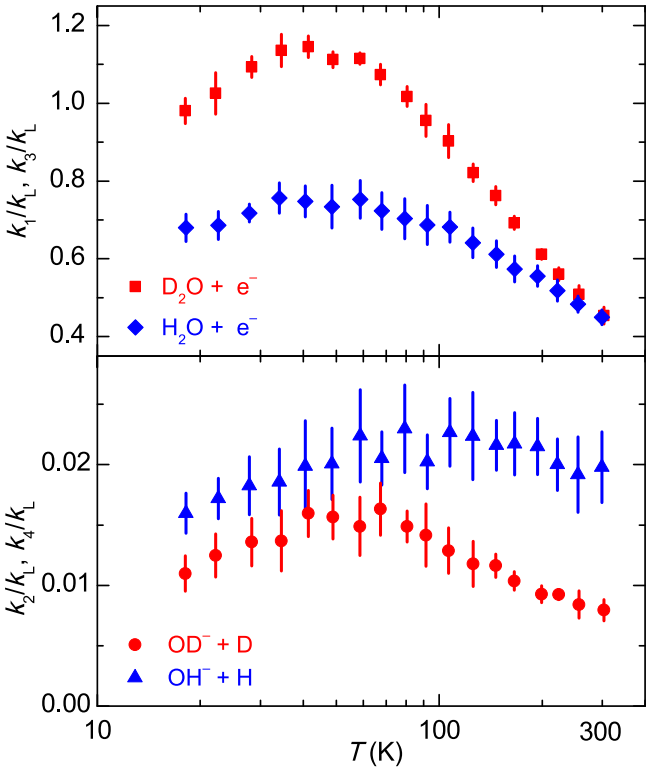


FIG. 5. Measured rate coefficients for the reaction of $O^-$ with $D_2$ and $H_2$ normalized to the corresponding Langevin collisional rate coefficients $k_L$. Upper panel: Normalized reaction rate coefficients $k_1$ and $k_3$ for associative detachment (1) and (3), respectively. Lower panel: Normalized reaction rate coefficients $k_2$ and $k_4$ for atom transfer (2) and (4), respectively. Statistical error bars, which are relevant for relative comparison, are indicated.

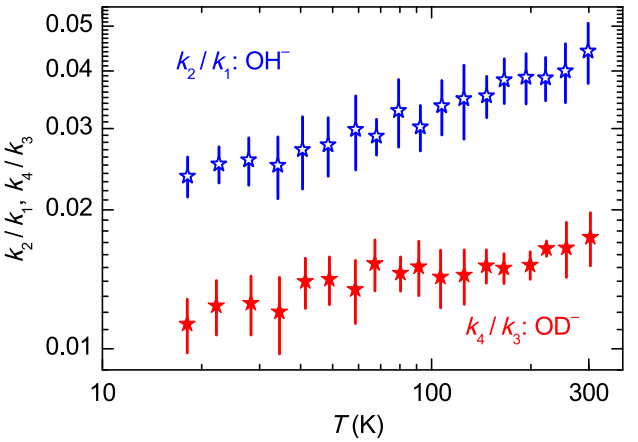


FIG. 6. Temperature dependencies of the branching ratios for the formation of $OH^-$ and $OD^-$ in the reaction of $O^-$ with $H_2$ or $D_2$, respectively. Statistical error bars are indicated.

in the temperature dependencies of the rate coefficients of the reactions of $O^-$ with $H_2$ and $D_2$. The difference of the reaction rate coefficients $k_2$ and $k_4$ for the atom transfer reactions with $H_2$ [reaction (2)] and $D_2$ [reaction (4)] is very pronounced. To highlight the difference between the rate coefficients $k_2$ and $k_4$ of the atom transfer reactions (2) and (4) the temperature dependencies of the corresponding branching ratios ($k_2/k_1$ and $k_4/k_3$) for the reaction channels leading to $OH^-$ or $OD^-$ are shown in Fig. 6. Note that in the temperature range 15–300 K the measured branching ratio for production of $OH^-$ is higher at least by a factor of 2 than the measured branching ratio for production of $OD^-$.

## IV. THEORY AND RESULTS OF CALCULATIONS

In order to understand the experimental results we performed the classical trajectory Monte Carlo simulation of the $O^- + H_2$ and $O^- + D_2$ collisions. We used the potential energy surfaces calculated previously using the multireference configuration interaction method [15]. We considered only the lowest electronic $1^2A'$ state, which connects the initial $O^- + H_2$ and the final $OH^- + H$ channels through the electron autodetachment region where neutral $H_2O$ can be formed (see Fig. 1 for the $O^- + D_2$ reaction). As discussed in detail in Refs. [15,16,35] there are other two states $1^2A''$, $2^2A'$ connected to the $O^- + H_2$ asymptote, however these two states cannot directly contribute neither to associative detachment nor to the $OH^- + H$ channel at low energies. There is nevertheless strong evidence (see [15] for detailed explanation) that the initial flux in those two states is transferred to the lowest state through a conical intersection near linear molecular configurations. The potential energy surface of the $1^2A'$ state was fitted with a sum of a large number of Gaussian functions, so that the error of the final fit does not exceed 10 meV in the regions energetically accessible in the $O^- + H_2$ collision at energies below 0.2 eV [43]. The autodetachment region was localized as a coordinate domain, where the calculated ground state of the neutral $H_2O$ molecule is located below the $1^2A'$ state of the anion. The resulting region was then fitted to an ellipsoid in the space of mutual atomic separations $R_{HH}$, $R_{OH1}$, and $R_{OH2}$ with semiaxes $a_{OH} = 0.85\,a_0$ and $a_{HH} = 1.65\,a_0$ ($a_0$ being the Bohr radius) [43].

To perform the classical trajectory Monte Carlo simulation we followed the procedure suggested by Karplus *et al.* [44]. Each trajectory was started in the asymptotic region of the $O^- + H_2$ channel with typical separation of colliding species of 30 $a_0$. The energy of the classical vibrational motion of the $H_2$ molecule was selected as the ground state of quantized motion. For each impact parameter $b$ the orientation and the vibrational phase of the $H_2$ molecule was selected randomly. For low temperatures studied in this work we assume that the $H_2$ molecule has initially zero angular momentum, but all degrees of freedom are included in classical dynamics. The classical trajectory was followed numerically with the fourth-order Runge-Kutta method until the trajectory was terminated in the autodetachment region (we assume that all these trajectories contribute to the associative detachment process) or the asymptote of either the $O^- + H_2$ or the $OH^- + H$ channel was reached. The same procedure was repeated for $10^3$–$10^4$ trajectories yielding the Monte Carlo estimate of reaction probability for each impact parameter $b$. We checked that the statistical error of Monte Carlo averaging is below 5%. The probability $P(E,b)$ of a certain process for a given energy $E$ and impact parameter $b$ is determined as a

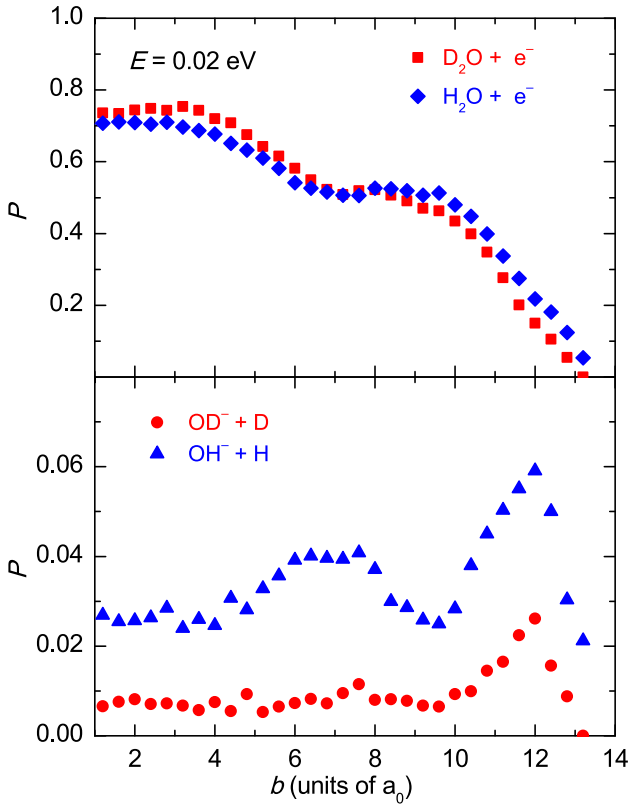


FIG. 7. Probabilities of associative detachment (upper panel) and atom transfer (lower panel) for the reactions of $O^-$ with $H_2$ and $D_2$ calculated as functions of the impact parameter $b$ at the collision energy $E = 20$ meV. The equivalent temperature $2E/3k_B$ is 155 K.

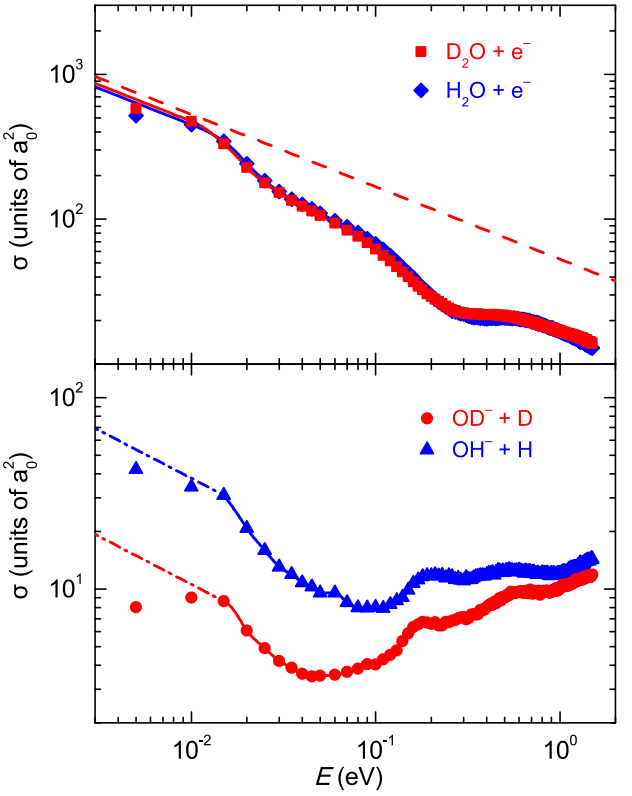


FIG. 8. Calculated energy dependencies of the cross sections for both channels of reactions of $O^-$ with $H_2$ and $D_2$. The energy scale of this plot corresponds to equivalent temperatures $2E/3k_B$ in the range of 23–15 500 K. Upper panel: The cross sections for associative detachment forming $H_2O$ and $D_2O$. The dashed straight line indicates the Langevin collisional cross section for $O^- + D_2$ (which differs from that of $O^- + H_2$ by about 1% due to differences in polarizabilities [45]). Lower panel: The cross sections for atom transfer leading to $OH^- + H$ and $OD^- + D$.

ratio of the number of trajectories ending in the corresponding channel to the number of all trajectories. The cross section $\sigma(E)$ as a function of energy of relative motion of $O^-$ and $H_2$ for each reaction is then obtained by integration of the respective probability

$$\sigma(E) = 2\pi \int_0^{b_{\max}} P(E,b)\, b\, db, \tag{8}$$

where $b_{\max}$ is the impact parameter where the reactions vanish and only the elastic $O^- + H_2$ channel remains. Note that zero-point energy of $H_2$ vibrations is not included in $E$ and adds to the total energy. Finally we calculated the reaction rate coefficients by averaging a product of velocity and cross section over the Maxwell-Boltzmann distribution of collision velocities. The same procedure was repeated for the $O^- + D_2$ system.

The typical results of our Monte Carlo simulations for $O^- + H_2$ and for $O^- + D_2$ are shown in Fig. 7 for the collision energy 20 meV. The graphs contain the dependence of the associative detachment and AT reaction probabilities on the impact parameter $b$, showing the relative number of trajectories ending in the autodetachment or $OH^-$ (or $OD^-$) regions. We can observe a typical decrease of the associative detachment probability with increasing $b$, while the reaction probability of AT increases before the final drop to zero. This is consistent with the assumption that the trajectories leading to the reaction have to squeeze in a narrow space between the central autodetachment and classically forbidden regions.

The calculated cross sections (8) for both processes in the reactions of $O^- + H_2$ and $O^- + D_2$ are plotted in Fig. 8. Although the cross sections are calculated for collisional energies up to 1.5 eV to calculate the rate coefficients at higher temperatures, we suspect that the detailed dynamics of nonadiabatic transitions in the conical intersection among all three $1^2A'$, $1^2A''$, and $2^2A'$ electronic states starts to play a role already at energies higher than 0.2 eV [15]. First few points of the cross section curve are considerably influenced by low accuracy of the potential energy fit. The error of the fit is approximately 10 meV which corresponds to abrupt change of behavior of the cross sections at this energy. Therefore we do not use the points below 15 meV in the calculation of the rates but we use the Langevin behavior $\sigma(E) \sim 1/\sqrt{E}$ to extrapolate the data as indicated by dash-dotted lines in Fig. 8. The dashed straight line in the upper panel indicates the Langevin cross section for the reaction of $O^- + D_2$.

The resulting rate coefficients for both channels of the reactions $O^- + H_2$ and $O^- + D_2$ are shown in Fig. 9 together with the present and some previous [22–24] experimental data.

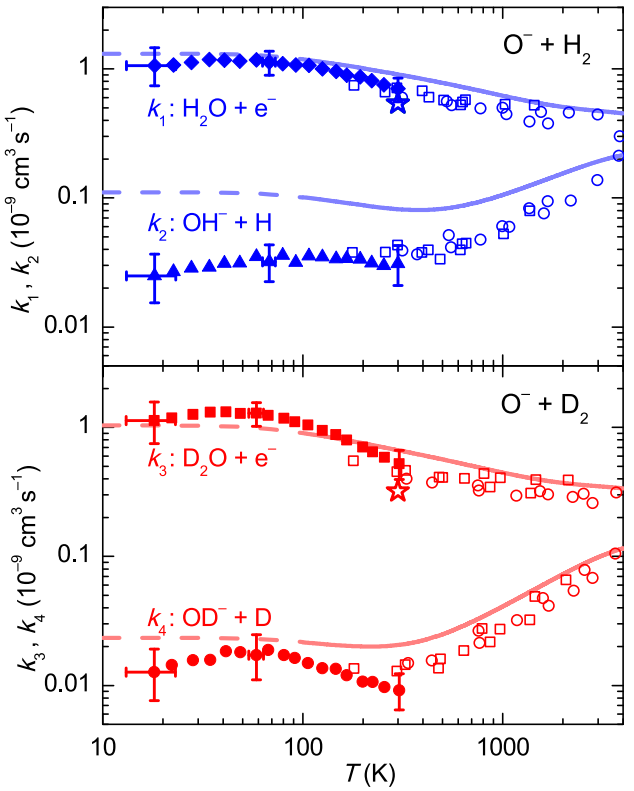


FIG. 9. Calculated and measured temperature dependencies of the reaction rate coefficients for both channels of the reactions of $O^-$ with $H_2$ and $D_2$. The experimental data points from the 22-pole instrument (full symbols) are compared with the results from the Monte Carlo simulations (lines) for both the hydrogenated (upper panel) and deuterated (lower panel) system. Open symbols indicate the experimental data of Viggiano *et al.* [24] (squares), McFarland *et al.* [22] (circles), and Jusko *et al.* [23] (stars). The part of the theoretical curve strongly dependent on the extrapolation of the calculated data is shown with dashed lines. The error bars with caps indicate the overall uncertainty for a few representative points.

The data that are influenced significantly by the cross section extrapolation below 10 meV are marked by dashed curves. Comparing the calculated and experimental rate coefficients in this figure, we see good qualitative agreement both in isotopic ratios of the AD and AT reaction processes and also in temperature dependencies. The absolute magnitude of the rate coefficients is off at most by a factor of 3, which is satisfactory considering the crudeness of the current model. First of all, it is a classical model and quantum effects may play an important role for such low energies, especially for the lighter $H_2$ molecule, which could explain why agreement of the computed rate $k_2$ with experiment is worse than for $k_4$. The crudeness of the model is also more pronounced for the AT reaction rates than for the AD rates because the AT rates are much smaller. Second, the nonadiabatic coupling near the conical intersection and the spin-orbit coupling are not taken into account. We plan to include these effects in future calculations. Moreover, we are currently using a crude model of the electron autodetachment. The local complex potential approximation could be implemented in the semiclassical procedure, however we do not have the data for the autodetachment widths at the moment. It has also been shown that the local complex potential model can be inappropriate [46], especially for polar molecules [47,48].

## V. CONCLUSIONS AND OUTLOOK

We measured the rate coefficients of associative detachment and H or D atom transfer in the reaction of $O^-$ with $H_2$ or $D_2$ at temperatures between 15 and 300 K (Fig. 4). At temperatures below 80 K the associative detachment rate coefficients for $H_2$ and $D_2$ are nearly identical, close to $1.2 \times 10^{-9}$ cm$^3$ s$^{-1}$. On the other hand, at 300 K, their values decrease below ≈50% of the respective Langevin collisional rate coefficients (Fig. 5). The measured atom transfer rate coefficients $k_2$ and $k_4$ are 2%–4% and 1%–2% of the corresponding overall reaction rate coefficients, respectively (see the branching ratios in Fig. 6). Comparison of the atom transfer data for the reactions with $H_2$ and $D_2$ normalized to the corresponding Langevin collisional rate coefficients (Fig. 5) indicates large difference between the temperature dependencies of the rate coefficients. The branching ratio $(k_2/k_1)$ for the reaction with $H_2$ is by a factor of 2 higher than the branching ratio $(k_4/k_3)$ for the reaction with $D_2$ (Fig. 6).

In order to understand the observed isotope effect, we carried out the classical trajectory Monte Carlo simulations of the $O^- + H_2$ and $O^- + D_2$ interactions using the newly calculated PES. From the calculated probabilities for both channels of both reactions as functions of the impact parameter $b$ and collision energy, we calculated the corresponding reaction cross sections (Fig. 8) and the rate coefficients for temperatures from 10 up to 4000 K (Fig. 9). Comparison of the calculated rate coefficients with the experimental data (Fig. 9) reveals good agreement in branching ratios, in the isotope effect, and in the shape of the temperature dependencies of the respective reaction rate coefficients.

The qualitative picture that emerges from the current classical trajectory simulation and from the shape of the potential energy landscape is following. At low energies the trajectories follow the initial channel potential valley, which is the most attractive along linear geometry alignment of $O^- + H_2$ or $D_2$. At short distances a barrier emerges in the linear geometry and $O^- + H_2$ or $D_2$ has to tilt in order to reach the autodetachment region through a saddle point. After passing the saddle point the autodetachment region represents a large obstacle in the path towards the atom transfer reaction channel. It is easier to reach the atom transfer channel for the $H_2$ molecule, which is lighter than $D_2$ and can tilt its orientation more easily. The reaction is also more probable for larger energies when the classically allowed region around the autodetachment ellipsoid becomes more voluminous. This enhances the reactivity of $H_2$, which has larger zero-point energy of vibrational motion than $D_2$. We checked that the difference in zero-point energy of the initial state of $H_2$ or $D_2$ is responsible for 50%–75% (depending on collision energy) of the isotopic effect.

It is interesting to note that the behavior of the temperature dependencies of the rate coefficients changes at temperatures around 300 K. This was not so clearly visible on the basis of

data from previous high temperature (drift tube) experiments. Only combination of drift tube data, our low temperature data and data obtained in our calculations give a better idea about the details of the $O^- + H_2$ and $O^- + D_2$ reactions. Further experimental and theoretical studies are needed. We are planning to study the differences in reactivity between ortho and para nuclear spin configurations of $H_2$ by means of the 22-pole trap combined with a para-hydrogen generator. For better understanding of these fundamental processes we are preparing studies of the reaction of $O^-$ with HD. We also plan to deepen our theoretical understanding of the studied reactions by taking into account the nonadiabatic coupling near the conical intersection and the spin-orbit coupling. Calculation of the autodetachment widths and implementation of the local complex potential approximation in the semiclassical procedure will be a subject of our future work.

## ACKNOWLEDGMENTS

This work was partly supported by the Czech Science Foundation (GACR P209/12/0233, GACR 16-17230S, GACR 17-19459S), and by the Charles University (GAUK 572214, 1144616, 1168216). We thank the Chemnitz University of Technology and the DFG for lending the 22-pole trap instrument to the Charles University. We want to thank Professor Gerlich for fruitful discussions.

[1] J. Liu, D. Sprecher, C. Jungen, W. Ubachs, and F. Merkt, J. Chem. Phys. **132**, 154301 (2010).
[2] P. Maksyutenko, T. R. Rizzo, and O. V. Boyarkin, J. Chem. Phys. **125**, 181101 (2006).
[3] J. R. Smith, J. B. Kim, and W. C. Lineberger, Phys. Rev. A **55**, 2036 (1997).
[4] C. Blondel, W. Chaibi, C. Delsart, C. Drag, F. Goldfarb, and S. Kröger, Eur. Phys. J. D **33**, 335 (2005).
[5] K. R. Lykke, K. K. Murray, and W. C. Lineberger, Phys. Rev. A **43**, 6104 (1991).
[6] K. Huber and G. Herzberg, *Molecular Spectra And Molecular Structure: Constants Of Diatomic Molecules*, Molecular Spectra and Molecular Structure, Vol. IV (Van Nostrand Reinhold, New York, 1979).
[7] D. S. Eisenberg and W. Kauzmann, *The Structure and Properties of Water* (Oxford University Press, Oxford, 1969).
[8] K. K. Irikura, J. Phys. Chem. Ref. Data **36**, 389 (2007).
[9] A. Dalgarno and R. A. McCray, Astrophys. J. **181**, 95 (1973).
[10] B. Marty, Earth Planet. Sci. Lett. **313–314**, 56 (2012).
[11] E. A. Bergin and E. F. van Dishoeck, Phil. Trans. R. Soc. London Sect. A **370**, 2778 (2012).
[12] L. I. Cleeves, E. A. Bergin, C. M. O. Alexander, F. Du, D. Graninger, K. I. Öberg, and T. J. Harries, Science **345**, 1590 (2014).
[13] D. Hollenbach, M. J. Kaufman, E. A. Bergin, and G. J. Melnick, Astrophys. J. **690**, 1497 (2009).
[14] H. Roberts and T. J. Millar, Astron. Astrophys. **361**, 388 (2000).
[15] P. Jusko, Š. Roučka, D. Mulin, I. Zymak, R. Plašil, D. Gerlich, M. Čížek, K. Houfek, and J. Glosík, J. Chem. Phys. **142**, 014304 (2015).
[16] K. Houfek and M. Čížek, Eur. Phys. J. D **70**, 107 (2016).
[17] D. M. Neumark, K. R. Lykke, T. Andersen, and W. C. Lineberger, Phys. Rev. A **32**, 1890 (1985).
[18] C. Blondel, C. Delsart, C. Valli, S. Yiou, M. R. Godefroid, and S. Van Eck, Phys. Rev. A **64**, 052504 (2001).
[19] L. A. Viehland, R. Webb, E. P. F. Lee, and T. G. Wright, J. Chem. Phys. **122**, 114302 (2005).
[20] M. Hejduk, P. Dohnal, J. Varju, P. Rubovič, R. Plašil, and J. Glosík, Plasma Sources Sci. Technol. **21**, 024002 (2012).
[21] I. Zymak, M. Hejduk, D. Mulin, R. Plašil, J. Glosík, and D. Gerlich, Astrophys. J. **768**, 86 (2013).
[22] M. McFarland, D. L. Albritton, F. C. Fehsenfeld, E. E. Ferguson, and A. L. Schmeltekopf, J. Chem. Phys. **59**, 6629 (1973).
[23] P. Jusko, Š. Roučka, R. Plašil, and J. Glosík, Int. J. Mass Spectrom. **352**, 19 (2013).
[24] A. A. Viggiano, R. A. Morris, C. A. Deakyne, F. Dale, and J. F. Paulson, J. Phys. Chem. **95**, 3644 (1991).
[25] S. T. Lee and J. M. Farrar, J. Chem. Phys. **111**, 7348 (1999).
[26] J. L. Mauer and G. J. Schulz, Phys. Rev. A **7**, 593 (1973).
[27] V. A. Esaulov, R. L. Champion, J. P. Grouard, R. I. Hall, J. L. Montmagnon, and F. Penent, J. Chem. Phys. **92**, 2305 (1990).
[28] D. J. Haxton, C. W. McCurdy, and T. N. Rescigno, Phys. Rev. A **75**, 012710 (2007).
[29] D. J. Haxton, T. N. Rescigno, and C. W. McCurdy, Phys. Rev. A **75**, 012711 (2007).
[30] H. Adaniya, B. Rudek, T. Osipov, D. J. Haxton, T. Weber, T. N. Rescigno, C. W. McCurdy, and A. Belkacem, Phys. Rev. Lett. **103**, 233201 (2009).
[31] D. J. Haxton, H. Adaniya, D. S. Slaughter, B. Rudek, T. Osipov, T. Weber, T. N. Rescigno, C. W. McCurdy, and A. Belkacem, Phys. Rev. A **84**, 030701 (2011).
[32] N. B. Ram, V. S. Prabhudesai, and E. Krishnakumar, J. Chem. Sci. **124**, 271 (2012).
[33] J. Fedor, P. Cicman, B. Coupier, S. Feil, M. Winkler, K. Głuch, J. Husarik, D. Jaksch, B. Farizon, N. J. Mason, P Scheier, and T. D. Märk, J. Phys. B: At. Mol. Opt. Phys. **39**, 3935 (2006).
[34] C. R. Claydon, G. A. Segal, and H. S. Taylor, J. Chem. Phys. **54**, 3799 (1971).
[35] H. J. Werner, U. Manz, and P. Rosmus, J. Chem. Phys. **87**, 2913 (1987).
[36] T. J. Millar, Plasma Sources Sci. Tech. **24**, 043001 (2015).
[37] D. Gerlich and G. Borodi, Faraday Discuss. **142**, 57 (2009).
[38] I. Zymak, P. Jusko, Š. Roučka, R. Plašil, P. Rubovič, D. Gerlich, and J. Glosík, Eur. Phys. J. Appl. Phys. **56**, 24010 (2011).
[39] D. Gerlich, P. Jusko, Š. Roučka, I. Zymak, R. Plašil, and J. Glosík, Astrophys. J. **749**, 22 (2012).
[40] R. Plašil, I. Zymak, P. Jusko, D. Mulin, D. Gerlich, and J. Glosík, Philos. Trans. R. Soc. London Ser. A **370**, 5066 (2012).
[41] D. Gerlich, R. Plašil, I. Zymak, M. Hejduk, P. Jusko, D. Mulin, and J. Glosík, J. Phys. Chem. A **117**, 10068 (2013).
[42] D. Mulin, Š. Roučka, P. Jusko, I. Zymak, R. Plašil, D. Gerlich, R. Wester, and J. Glosík, Phys. Chem. Chem. Phys. **17**, 8732 (2015).

[43] J. Táborský, Master thesis, Charles University, Faculty of Mathematics and Physics, Prague, 2016 .
[44] M. Karplus, R. N. Porter, and R. D. Sharma, J. Chem. Phys. **43**, 3259 (1965).
[45] Y. Y. Milenko, L. V. Karnatsevich, and V. S. Kogan, Physica **60**, 90 (1972).
[46] R. J. Beiniek, J. Phys. B: At. Mol. Phys. **13**, 4405 (1980).
[47] S. Živanov, M. Allan, M. Čížek, J. Horáček, F. A. U. Thiel, and H. Hotop, Phys. Rev. Lett. **89**, 073201 (2002).
[48] S. Živanov, M. Čížek, J. Horáček, and M. Allan, J. Phys. B: At. Mol. Opt. Phys. **36**, 3513 (2003).